

Modeling dislocation sources and size effects at initial yield in continuum plasticity

Saurabh Puri ^a, Anish Roy ^b, Amit Acharya ^a, Dennis Dimiduk ^c

^a Civil and Environmental Engineering, Carnegie Mellon University, Pittsburgh, PA 15213, U.S.A

^b Materials Engineering Center, DOW Chemical Company, Terneuzen, The Netherlands

^c Air Force Research Laboratory, Materials and Manufacturing Directorate, AFRL/MLLM Bldg. 655, 2230 Tenth Street, Wright Patterson, AFB, OH 45433-7817, U. S. A.

Abstract

Size effects at initial yield (prior to Stage II) of micron sized specimens are modeled within a continuum model of plasticity. Two different aspects are considered here: a) specification of a density of dislocation sources that represent the emission of dislocation dipoles, and b) the presence of an initial, spatially inhomogeneous excess dislocation (ED) content. Discreteness of the source distribution appears to lead to a stochastic response in stress-strain curves, with the stochasticity diminishing as the number of sources increases. Variability in stress-strain response due to variations of source distribution is also shown. These size effects at initial yield are inferred to be due to physical length scales in dislocation mobility and the discrete description of sources that induce internal-stress-related effects, and not due to length-scale effects in the mean-field strain-hardening response (as represented through a constitutive equation).

Keywords: Continuum plasticity, Dislocations, Finite elements.

1. Introduction

There is a considerable body of experimental evidence that demonstrates that plastic deformation in FCC and other crystalline solids is size dependent at length scales of the order of tens of microns and smaller (e.g. Fleck et al., 1994; Ma and Clarke, 1995; Stolken and Evans, 1998). Research has suggested that this behavior can be either an effect of constraint imposed on dislocation motion from grain boundaries or internal interfaces or an effect of excess dislocation density resulting from similar externally imposed constraints. However, recently, experiments performed on unconstrained single crystals demonstrated strong size effects at initial yield (including a hardening phenomenon at small strains) as well (Uchic et al., 2004; Dimiduk et al., 2005; Greer et al., 2005). This observed phenomena was modeled within a 2d Discrete Dislocation (DD) framework in Deshpande et al. (2005), Benzerga et al. (2005), Benzerga and Shaver (2006) and Balint et al. (2006) and, more recently using 3d DD techniques. From those studies one may develop a perception that it is not possible to model such effects within a continuum framework.

In this paper we examine the question of how dislocation sources may be modeled in continuum plasticity. We find the answer to be affirmative and use the strategy to demonstrate size effects at initial yield within the context of a recently proposed continuum theory, namely, Phenomenological Mesoscopic Field Dislocation Mechanics (PMFDM) (Acharya and Roy, 2006). Results obtained from a finite-element implementation of the theory have been shown to reasonably account for plasticity at mesoscopic scales. Physical length scales exist in the theory and size-affected strain hardening has been demonstrated successfully (Roy and Acharya, 2006). In this paper we shall specifically discuss size effects at initial yield based on two continuum-level mechanisms. First, size effects are demonstrated in specimens having a predefined pattern

of statistical dislocation (SD) sources. For the second mechanism, simulations are performed on specimens having an initial, spatially inhomogeneous excess dislocation (ED) distribution.

The paper is organized as follows: in Section 2, a brief description of the governing equations of PMFDM is presented. Section 3 involves discussion of modeling strategy and results so obtained.

The paper ends with some concluding remarks in Section 4.

A note regarding terminology: henceforth, given a scale of resolution l , we refer to the spatial average of Nye's (1953) dislocation-density tensor over a volume l^3 around a point as the *Excess Dislocation* (ED) density tensor at that point. Nye's tensor being a tensorial quantity, the dislocations that are averaged out in this process due to cancellation in sign form a density that we refer to as the *Statistically Distributed Dislocation* (SD) density. Thus, the difference of local value of Nye's tensor field and its spatial average (ED) is referred to as SD.

2. Theory

The Phenomenological Mesoscopic Field Dislocation Mechanics (PMFDM) theory (Acharya and Roy, 2006) results from an elementary space-time averaging of the equations of Field Dislocation Mechanics (Acharya 2001, 2003, 2004). It admits constitutive hypotheses on elasticity, the mean (i.e. space-time average) of signed velocity of dislocation segments (that may be associated with the velocity of mean ED), and the mean slip rate produced by SD. The phenomenology introduced in the model is meager, with the qualitative predictions of the model not depending upon the phenomenological assumptions. The essential equations of PMFDM are summarized below¹.

The (symmetric) stress tensor \mathbf{T} satisfies

¹ For motivation behind the formulation the reader is referred to the work of Acharya and Roy (2006)

$$\begin{aligned} \mathbf{T} &= \mathbf{C} : \mathbf{U}^e \\ \text{div} \mathbf{T} &= \mathbf{0} \end{aligned} \quad (1)$$

along with standard traction/displacement boundary conditions. \mathbf{C} is the possibly anisotropic fourth order tensor of linear elastic moduli and \mathbf{U}^e is the elastic distortion tensor defined as

$$\mathbf{U}^e = \text{grad} \mathbf{u} - \mathbf{U}^p. \quad (2)$$

In the above equation, \mathbf{u} is the total displacement field and \mathbf{U}^p is the plastic distortion tensor which is decomposed uniquely into compatible and incompatible parts as

$$\mathbf{U}^p = \text{grad} \mathbf{z} - \boldsymbol{\chi}. \quad (3)$$

Thus, the elastic distortion tensor may be rewritten as,

$$\mathbf{U}^e = \text{grad}(\mathbf{u} - \mathbf{z}) + \boldsymbol{\chi}, \quad (4)$$

where the field $\boldsymbol{\chi}$ cannot be written as a non-trivial gradient. The incompatible part, $\boldsymbol{\chi}$, is given by

$$\begin{aligned} \text{curl} \boldsymbol{\chi} &= \boldsymbol{\alpha} \\ \text{div} \boldsymbol{\chi} &= \mathbf{0} \\ \boldsymbol{\chi} \mathbf{n} &= \mathbf{0} \text{ on } \partial B \end{aligned} \quad (5)$$

where, $\boldsymbol{\alpha}$ is space-time averaged dislocation density tensor field and \mathbf{n} is the unit normal on the boundary ∂B of the body. The vector field \mathbf{z} whose gradient represents the compatible part of \mathbf{U}^p obeys the relation

$$\begin{aligned} \text{div}(\text{grad} \dot{\mathbf{z}}) &= \text{div}(\boldsymbol{\alpha} \times \mathbf{V} + \mathbf{L}^p) \\ (\text{grad} \dot{\mathbf{z}}) \mathbf{n} &= (\boldsymbol{\alpha} \times \mathbf{V} + \mathbf{L}^p) \mathbf{n} \text{ on } \partial B, \end{aligned} \quad (6)$$

where V and L^p need to be specified constitutively. V represents the velocity of the ED and L^p has the physical meaning of representing that part of the total slip strain rate which is not represented by the slipping produced by the averaged signed dislocation density (ED). The value of $\dot{\alpha}$ is prescribed at an arbitrarily chosen point of the body and in our case is assumed to vanish without loss of generality. Finally the temporal evolution of the dislocation-density tensor field is prescribed as

$$\dot{\alpha} = -\text{curl } \mathbf{S}, \quad (7)$$

where \mathbf{S} is the averaged slipping distortion (slip rate) defined as

$$\mathbf{S} := \alpha \times V + L^p. \quad (8)$$

2.1. Boundary Condition on Surface Flow

Equation (7) admits boundary conditions on the dislocation flow (Acharya and Roy, 2006). In general, a natural boundary condition of the form

$$\mathbf{S} \times \mathbf{n} = \Phi, \quad (9)$$

where Φ is a (second-order tensor valued) specified function of time and position along the boundary satisfying the constraint $\Phi \mathbf{n} = \mathbf{0}$, is appropriate to model controlled flow at the boundary. A rigid boundary with respect to slipping may be represented with a zero flow boundary condition

$$\mathbf{S} \times \mathbf{n} = \mathbf{0} \quad (10)$$

on the entire boundary. Imposing such a boundary condition can lead to the development of shocks or discontinuities. A less restrictive boundary condition is the imposition of the dislocation flux, $\alpha(V \cdot \mathbf{n})$, on inflow points of the boundary (where $V \cdot \mathbf{n} < 0$), along with a

specification of $\mathbf{L}^p \times \mathbf{n}$ on the entire boundary. This condition allows free exit of dislocations without any added specification.

2.2. Constitutive Specification

Constitutive specifications for the dislocation-velocity vector, \mathbf{V} , and the slip-distortion rate due to SDs, \mathbf{L}^p , are required. Simple choices motivated by conventional plasticity and the thermodynamics of PMFDM (Acharya and Roy, 2006) are

$$\begin{aligned}\mathbf{L}^p &= \dot{\gamma} \frac{\mathbf{T}'}{|\mathbf{T}'|} \quad ; \quad \dot{\gamma} \geq 0, \\ \mathbf{V} &= v \frac{\mathbf{d}}{|\mathbf{d}|} \quad ; \quad v \geq 0,\end{aligned}\tag{11}$$

where, \mathbf{T}' is the stress deviator, $\dot{\gamma}$ and v are non-negative functions of state representing the magnitudes of the SD slipping rate and the averaged ED velocity, respectively. The direction of the dislocation velocity is defined by

$$\begin{aligned}\mathbf{d} &:= \mathbf{b} - \left(\mathbf{b} \cdot \frac{\mathbf{a}}{|\mathbf{a}|} \right) \frac{\mathbf{a}}{|\mathbf{a}|}, \\ \mathbf{b} &:= \mathbf{X}(\mathbf{T}'\boldsymbol{\alpha}) \quad ; \quad b_i = e_{ijk} T'_{jr} \alpha_{rk} \quad ; \quad \mathbf{a} := \mathbf{X}(\text{tr}(\mathbf{T})\boldsymbol{\alpha}) \quad ; \quad a_i = \left(\frac{1}{3} T_{mm} \right) e_{ijk} \alpha_{jk}.\end{aligned}\tag{12}$$

Thermodynamics indicates \mathbf{b} as the driving force for \mathbf{V} ; the definition of \mathbf{d} is to ensure pressure independence of plastic straining in the model. We choose a power law relation for $\dot{\gamma}$ as

$$\dot{\gamma} = \dot{\gamma}_0 \left(\frac{|\mathbf{T}'|}{\sqrt{2}g} \right)^{\frac{1}{m}},\tag{13}$$

where, m is the macroscopic rate-sensitivity of the material, g is the strength of the material, and $\dot{\gamma}_0$ is a reference strain rate. The expression for v is assumed to be

$$v(\text{state}) = \eta^2 b \left(\frac{\mu}{g} \right)^2 \dot{\gamma}(\mathbf{T}', g), \quad (14)$$

where μ is the shear modulus, b the Burgers vector magnitude and $\eta = 1/3$ a material parameter.

The strength of the material is assumed to evolve according to

$$\dot{g} = \left[\frac{\eta^2 \mu^2 b}{2(g - g_0)} k_0 |\boldsymbol{\alpha}| + \theta_0 \left(\frac{g_s - g}{g_s - g_0} \right) \right] \{ |\boldsymbol{\alpha} \times \mathbf{V}| + \dot{\gamma} \}, \quad (15)$$

where g_s is the saturation stress, g_0 is the yield stress, and θ_0 is the Stage II hardening rate. The material parameters $g_s, g_0, \mu, b, \dot{\gamma}_0, m$ are known from conventional plasticity (Voce Law and power-law hardening). Consequently, k_0 is the only extra parameter that needs to be fitted and can be obtained from experimental grain-size dependence of flow stress results, as shown in Acharya and Beaudoin (2000) and Beaudoin et al. (2000).

The finite-element discretization for the above system of equations is discussed in Roy and Acharya (2006). Here we only summarize the finite-element discretization of equation (7), which has an extra term in the weak formulation corresponding to the LSFEM discretization of the inflow boundary condition on $\boldsymbol{\alpha}$ (Varadhan et al., 2006).

In the following expression, the symbol $\delta(\cdot)$ represents a variation (or test function) associated with the field (\cdot) in a suitable class of functions. An increment of time $[t, t + \Delta t]$ is considered, and fields without any superscripts refer to values at $t + \Delta t$ and those with the superscript t

refer to values at time t . All spatial fields are discretized by first-order, 8-node (three-dimensional), isoparametric brick elements. A mixed Forward-Backward Euler scheme is adopted as

$$\begin{aligned}
& \int_B \delta\alpha_{ij} (\alpha_{ij} - \alpha_{ij}^t) dv - \Delta t \int_B [\delta\alpha_{ij,k} \alpha_{ij} v_k^t - \delta\alpha_{ij,k} \alpha_{ik} v_j^t] dv \\
& - \Delta t \int_B \delta\alpha_{ij} s_{ij}^t dv + \Delta t \int_{\partial B_i} \delta\alpha_{ij} F_{ij} da \\
& + \Delta t \int_{\partial B_o} \delta\alpha_{ij} \alpha_{ij}^t (v_k^t n_k) da - \Delta t \int_{\partial B} \delta\alpha_{ij} \alpha_{ik}^t n_k v_j^t da \\
& - \Delta t \int_B \delta\alpha_{ij,k} e_{jkl} L_{il}^p dv + \Delta t \int_{\partial B} \delta\alpha_{ij} e_{jkl} L_{il}^p n_k da \\
& + \int_{B_{\text{interiors}}} A_{ri} (\delta\alpha_{ri} + \Delta t [\delta\alpha_{ri,j} v_j^t + \delta\alpha_{ri} v_{j,j}^t - \delta\alpha_{rj,j} v_i^t - \delta\alpha_{rj} v_{i,j}^t]) dv \\
& + \Delta t \int_{\partial B_i} \delta\alpha_{ij} (F_{ij} - \alpha_{ij}^t (v_k^t n_k)) da = 0
\end{aligned} \tag{16}$$

where

$$A_{ri} = \alpha_{ri} - \alpha_{ri}^t + \Delta t [\alpha_{ri,j}^t v_j^t + \alpha_{ri}^t v_{j,j}^t - \alpha_{rj,j}^t v_i^t - \alpha_{rj}^t v_{i,j}^t - s_{ri}^t + e_{ijk} L_{rk,j}^p]. \tag{17}$$

F is the prescribed flux on the inflow boundary (∂B_i), ∂B_o is the set of outflow/neutral points of the boundary where $V \cdot \mathbf{n} \geq 0$ and $B_{\text{interiors}}$ refers to the union of the element interiors. $\delta\alpha_{ij}$ is arbitrary up to satisfying any prescribed essential boundary conditions. The underlined term in (16) is an additional term that enters the discretization for excess dislocation-density evolution for all the computations in this paper over those described in Roy and Acharya (2006). The scheme is consistent even without the addition of this term; numerical experiments show a better imposition of inflow boundary conditions with its inclusion.

3. Results and Discussion

Unless otherwise mentioned, material parameters used for all the computational experiments are $b = 4.05 \times 10^{-4} \mu\text{m}$, $m = 1.0$, $g_s = 161 \text{ MPa}$, $g_0 = 17.3 \text{ MPa}$, $\theta_0 = 392.5 \text{ MPa}$ and $k_0 = 20.0$.

The reference strain rate is $\dot{\gamma}_0 = 1 \text{ sec}^{-1}$. Isotropic elastic constants of the representative material, Aluminum, are $E = 62.78 \text{ GPa}$, $\nu = 0.3647$, where E is the Young's modulus and ν is the Poisson's ratio.

A comment on the rate sensitivity value is in order. Our intent here is to model a situation where dislocations move in unobstructed, free-flight mode in large parts of the body. Under these circumstances, and with the understanding that rate-insensitivity is a manifestation of very fast motions homogenized in time with near stationary events, it is only reasonable to utilize a rate-sensitivity parameter value representative of linear drag in our simulations.

The initial conditions corresponding to the field equations mentioned in Section 2 are as follows.

For the \mathbf{u} field we assume $\mathbf{u}|_{t=0} \equiv \mathbf{0}$, which is a physically natural initial condition on the displacement field. Unless otherwise mentioned, we assume that the body is initially ED-free which translates to $\boldsymbol{\alpha}|_{t=0} \equiv \mathbf{0}$. The initial condition on the $grad \mathbf{z}$ field is obtained from solving (1) and (5) with $\mathbf{u}|_{t=0} \equiv \mathbf{0}$ and the value of \mathbf{z} set to zero at a single arbitrary point in the body.

Time-dependent simple-shearing solutions are studied numerically. The imposed boundary conditions corresponding to such a loading are as follows: displacements on the bottom face are constrained in all three directions while those on the top, left and right faces are constrained in the x_2, x_3 directions only (Figure 1). The front and back faces are displacement-constrained in the x_3 direction and traction free in x_1, x_2 direction. The displacements corresponding to a simple shear strain are prescribed through the kinematic boundary condition

$$u_1(x_1, x_2, x_3, t) = d(x_2) \dot{\Gamma} t \quad (18)$$

on the nodes of the left, right, top and bottom faces. Here, $d(x_2)$ is the height, from the bottom of the cube, of the point with coordinates (x_1, x_2, x_3) . Γ is the average engineering shear strain given by the ratio of the applied horizontal displacement of the top surface to the cube height; $\dot{\Gamma}$ is an applied shear strain rate of 1 sec^{-1} , and t is time.

All computations are performed on one of two desktop machines with 2GB and 8GB RAM, respectively. In the interpretation of results, symbol τ refers to the nominal (reaction) shear traction on the top surface of the sample.

3.1. Dislocation source distribution

The effect of physical dimensions of the simulation cell on the initial yield strength of the sample having a predefined distribution of SD sources is described in this section. First we discuss how a Frank Read source is grossly represented in our framework. In general, a Frank Read source produces dislocation loops that cannot be sensed if their size is less than the scale of resolution. However, once the loop expands up to the scale of resolution, it can be sensed as demonstrated in Figure 2a. In order to numerically simulate (SD) dislocation sources in the framework of PMFDM, the size of the region representing a source is assumed to be greater than or equal to the scale of resolution (Figure 2b). In the interior of the source region there are no EDs due to cancellation in signs during averaging. This corresponds to the physical situation of the dislocation loop not being sensed when its size is smaller than the scale of resolution. The plastic strain rate corresponding to the motion of these unresolved dislocations, however, is sensed, and is taken into account through L^p . At the interface between slipped and un-slipped region, EDs are observed due to the gradient in plastic strain rate (7)-(8). This observation corresponds to the

physical definition of a dislocation loop being sensed when its size equals or exceeds the scale of resolution. A simple test is performed to demonstrate this idea. Consider a cubical specimen of edge length of $1.0\mu\text{m}$ and discretized into a finite element grid. The element at the center is the dislocation source region, as shown in Figure 2b. The sample is unstressed and ED free initially, with some SD content in the source region. Displacement boundary conditions corresponding to a simple shear strain of 0.1% are imposed. With the onset of plasticity in the source region, edge dislocations (α_{13}) of opposite signs generated at the sub-grid scale of resolution cancel each other, resulting in zero dislocation density inside the source region, though a change in the magnitude of L_{12}^p values corresponding to these cancelled dislocations is observed. Since L^p is zero in non-slipped regions, a gradient in L_{12}^p develops at the interfaces of the slipped and non-slipped regions which in turn leads to the generation of α_{13} through (7), as shown in Figure 2c. The generated α_{13} density contributes to flow in the non-source-containing grid elements.

Now we discuss size effects at initial yield in samples having a predefined distribution of dislocation sources. Two cubical samples are considered having edge lengths of $0.6\mu\text{m}$ and $3.0\mu\text{m}$ and a spatial distribution of dislocation sources as shown in Figure 3. Displacement boundary conditions corresponding to an engineering simple shearing strain of 0.3% are imposed on the samples as in (18). First, experiments were performed in the context of conventional plasticity theory. Conventional plasticity may be recovered from PMFDM by setting $\alpha = \theta$ for all times and replacing (2) with

$$\mathbf{U}^e = \text{grad } \mathbf{u} - \mathbf{U}^p ; \dot{\mathbf{U}}^p = \mathbf{L}^p \quad (19)$$

Since, $\alpha = \theta$ in the conventional plasticity framework, non-source regions are elastic in nature. A size effect is observed for this case as shown in Figure 4, with smaller being harder. It can be

inferred from dimensional analysis that in the case of a homogeneous material, there is no length scale in the classical plasticity theory and hence it is not possible to predict size effects in this framework. However, a length scale emerges when a body consisting of discrete dislocation sources is considered. Dimensional analysis of τ yields,

$$\tau = \mu \Phi \left(\frac{\theta_0}{\mu}, \frac{g_s}{\mu}, \frac{g_0}{\mu}, \frac{\dot{\Gamma}}{\dot{\gamma}_0}, m, \Gamma, \frac{s}{H} \right), \quad (20)$$

where H denotes the dimension of the body, s is a representative measure of the distance between the sources (strictly speaking, the size of the sources should also enter as another length-scale parameter), and Φ is a dimensionless function of the arguments shown. It can be deduced from the relation above that if s is kept the same and H is changed, a difference in average response is expected. Thus, it is the spatial layout of dislocation sources that introduces a physical length scale in classical plasticity theory which is otherwise absent. However, the magnitude of that size effect on an average response utilizing discrete sources in an otherwise conventional elasto-plastic material falls short of what is qualitatively observed in experiment, indicating the existence of other scale effects and the need for better theory. Nonetheless, this same phenomenology of dislocation sources carries in PMFDM, but now with a greater effect because of the generation of ED at all spatial discontinuities of flow (such as source and non-source grid elements) and its transport, as well as its accurate accounting in stress response via (1)-(5).

The same numerical experiment is now performed with PMFDM. Accordingly, two cubical samples having edge lengths of $0.6\mu\text{m}$ and $3.0\mu\text{m}$ and a spatial distribution of dislocation sources as shown in Figure 3, are considered. *The area density of sources is identical (0.1) in both samples.* The displacement boundary conditions corresponding to a simple shear strain of 0.8%

are applied through (18). The non-source regions can behave in a plastic manner when ED content is transported through them; however, there is no SD slip rate in these regions.

The average shear stress-strain response, in Figure 5a, shows that initial yield strength strongly depends on the specimen size with smaller being harder. The size effect is maintained throughout the process of deformation in qualitative agreement with experimentally observed trends (Dimiduk et al., 2005; Greer et al., 2005). A significant stress drop is observed in our results which is absent in the experimental results (Uchic et al., 2004). This is due to the fact that numerical experiments performed here correspond to displacement control whereas the experimental results presented in Uchic et al. (2004) and Dimiduk et al. (2005) involved mixed (load and displacement) control. The applied load was not allowed to decrease during the experiments performed by Uchic et al. (2004) and Dimiduk et al. (2005) and thus, stress drops are not observed. In order to understand the cause of size-effect in the current framework, dimensional analysis of the applied, (reaction) nominal stress τ is performed which implies the following relation,

$$\tau = \mu \Phi \left(\frac{\theta_0}{\mu}, \frac{g_s}{\mu}, \frac{g_0}{\mu}, \frac{\dot{\Gamma}}{\gamma_0}, \frac{b}{H}, \alpha_0 H, m, \Gamma, k_0, \eta, \frac{s}{H} \right) \quad (21)$$

where, α_0 is a representative measure of the magnitude of the initial dislocation density field, s is a representative measure of the distance between sources and Φ is a dimensionless function of the arguments shown. The dimensionless arguments $b/H, \alpha_0 H, s/H$ introduce a dependence of average response on the Burgers vector of the material, the geometric proportion of the body, the initial dislocation density and the layout of sources. In these series of tests, the response is independent of $\alpha_0 H$ as the specimens were initially ED-free. Due to the change in spatial distribution of dislocation sources (with associated changes in ED generation), internal stresses

may change. Thus, s/H corresponds to the effect of internal stresses of dislocation distributions on average response. The argument (b/H) corresponds to the size effects due to dislocation mobility (14) and strain hardening (15). To evaluate the dependence of the response on internal length scale in strain hardening, the following equation is used for hardening rate instead of (15),

$$\dot{g} = \theta_0 \left(\frac{g_s - g}{g_s - g_0} \right) \{ |\boldsymbol{\alpha} \times \mathbf{V}| + \dot{\gamma} \}. \quad (22)$$

Use of such an equation removes all excess hardening by the ED evolution and interactions. Nonetheless, significant size effects are observed as shown in Figure 5b. Thus, from these sets of computational experiments it may be inferred that the size effect at initial yield in PMFDM is primarily due to length scales induced by i) a discrete SD source distribution and ii) the ED mobility, but not due to strain hardening in the mean-field or Stage II sense. This finding is qualitatively consistent with the recent reports by Norfleet et al. (2008), and Rao et al. (2008), both of which show a potent hardening mechanism for microcrystal deformation that is associated with the instantaneous mobile dislocation density relative to the imposed loading conditions. Further, the result does not preclude other hardening phenomena, such as the absence of sources as suggested by Greer et al. (2005), or the hardening of sources as suggested by Parthasarathy et al. (2006), from providing alternate or additional hardening mechanisms, respectively.

3.1.1. Effect of dynamic instability

To study the possibility of dynamical sensitivity of the stress-strain response at initial yield, additional numerical experiments were performed, each corresponding to a small perturbation of the order of 10^{-15} μm in the boundary condition for displacement. The spatial distribution of

sources is assumed to be similar to that used in section 3.1. It is observed that this small magnitude of perturbation in boundary condition results in a significant difference in the stress-strain response as shown in Figures 6a and 6b. There is about 34% variation in the shear stress at 0.8% applied strain for the sample having an edge length of $0.6\mu\text{m}$ and 16% for the sample having a $3.0\mu\text{m}$ edge length. The mean shear stress-strain response for each sample size is shown in Figure 6c. The mean values show a significant size dependence with smaller being harder.

The mechanical response at macroscopic scale is insensitive to minor perturbations. At the macroscopic scale, sources are considered to be present everywhere in the body. Motivated by this fact, numerical experiments were performed with sources present everywhere in the body, i.e. L^p is set active in the entire sample. The four simple shear experiments with varying boundary condition perturbations were performed on the small and big samples. It was observed that the stress-strain response in case of plastically unconstrained grains up to 0.8% simple shear strain is insensitive to such perturbation in the boundary conditions.

From these experiments and results presented in Roy and Acharya (2006) pertaining to effect of size on stability of stress-strain response in PMFDM, one may infer that i) discreteness in source distribution and ii) decreasing sample size lead to dynamical sensitivity to perturbations in this model. Interestingly, there are experimental observations of drastically different responses in samples of same size when subjected to a prescribed deformation (Uchic et al., 2004). However, it is not yet possible to deduce from those experiments the degree to which such variation results from differences in initial dislocation configurations and how much may result from small perturbations in the testing. The existence of such intrinsic instability in flow response also emphasizes the importance of the stochastic nature of the material response and the need to average over large numbers of samples to glean the typical material behavior at small scales.

3.1.2. Variation of microstructure

It was deduced from dimensional analysis performed in section 3.1 that the stress-strain response of PMFDM material depends upon the dimensionless argument s/H . Here we investigate the effect of changes in the spatial distribution of sources in a specimen of fixed size containing a fixed source density. Calculations for a cubic sample having an edge length of $3\mu\text{m}$ were performed with three different patterns of source distribution, as shown in Figure 7. No perturbations were imposed in this case. Figure 7 shows that average stress at 0.8% applied strain varies approximately from 43 MPa to 180MPa with varying source pattern. This demonstrates the variation of mechanical response of same-sized specimens with a change in microstructure.

Since specimens (a) and (c) are geometrically symmetric (if sample (a) is rotated by 180 degrees about the x_3 direction, it will be geometrically similar to sample (c)), the intuitive expectation is to get same response in these cases. It is evident from Figure 7 that top face of (a) corresponds to the bottom face of (c) after rotation. Reaction forces, however, are measured at the top face of all samples. The cause for this difference in the reaction force for the two different source patterns is due to the presence of non-zero tractions in the 1-direction on left and right faces of the cube due to the imposed displacement boundary conditions for simple shear. Accordingly, the reaction forces on the top need not be equal in magnitude to the reaction forces at the bottom of the sample. The horizontal reaction force on the top face of (a) (bottom face of (a)) was indeed identical to the horizontal reaction at the bottom face of (c) (top face of (c)) as required by symmetry. The top and bottom face reactions would have to be equal in magnitude from statics

for both (a) and (c) if the side faces of the cube were traction free in the 1-direction; this was verified in our numerical experiments.

3.2. Size effects due to initial ED distribution

Low energy dislocation microstructures are observed in materials. Such structures frequently consist of an array of like-signed dislocations having a low-energy arrangement, such as a tilt or twist boundary. Here we investigate the variation of initial yield strength in samples having a predefined spatial distribution of initial ED density of a common sign. Two cubical samples having edge lengths of $0.6\mu\text{m}$ and $3\mu\text{m}$ are considered. The spatial distribution of initial ED density is shown in Figure 3 for an edge-dislocation density of $\alpha_{23} = -2.025 \times 10^{-3} \mu\text{m}^{-1}$ prescribed on the nodes of shaded elements. In order to obtain an equilibrium state of initial ED density distribution, samples are relaxed in time without any external load. The volume average of $|\alpha|$ is used as a measure of ED content in the sample. Equilibrium is considered to be attained at $t = 0.03\text{sec}$ when this measure attains a constant value with respect to time, as shown in Figure 8a. The strength of the material is assumed to be constant throughout the deformation process, i.e. $\dot{g} = 0$ in (15). Once equilibrium is attained, simple shear boundary conditions corresponding to a strain of 0.3% are imposed on the samples. The average shear stress at 0.3% strain for the sample having an edge length of $0.6\mu\text{m}$ is 2.5 times higher than that of sample having a $3\mu\text{m}$ edge length as shown in Figure 8b. Next, a similar test was performed with an initially-prescribed ED density of same magnitude and opposite in sign. A reversed size effect is observed in this test wherein the larger sample shows a harder response (Figure 8b). One can infer from the dimensional analysis performed in section 3.1 (21), that the average response of the material depends upon $\alpha_0 H$ for these cases. With a prescribed α_0 among different sized specimens a size effect is expected but it is not possible to predict the sense of size effect based

on dimensional analysis alone. Due to the complexity and difference in initial ED distribution in these examples, a simpler problem is studied to understand the variation in the sense of size effect depending on the sign of initial ED density. For this simpler case, an initial excess edge-dislocation density $\alpha_{23} = 2.025 \times 10^{-3} \mu\text{m}^{-1}$ is prescribed at the center of two cubic samples having edge lengths of $0.6 \mu\text{m}$ and $3 \mu\text{m}$, as shown in Figure 9. The samples are relaxed in time to obtain corresponding equilibrated ED arrangements. Then, displacement boundary conditions corresponding to an engineering simple shearing strain of 0.3% are imposed on the sample. The average shear stress-strain response demonstrates that the smaller sample is indeed harder than the large one. However, a reversed size effect is observed with a change in sign of initial dislocation density (Figure 9). This phenomenon is explained as follows.

Consider a traction free finite cubical block containing a dislocation. In order to understand the resulting stress distribution in the block, we first note that the equations for determining the stress field of a specified ED field in PMFDM are linear; thus superposition applies. Consider now the stress field of a dislocation in an infinite medium, situated as in Figure 9. This infinite medium stress field naturally induces tractions on the surface of the finite crystal. Thus, image tractions equal in magnitude and opposite in sign of those induced by the dislocation need to be present on the external surface of the block to satisfy the traction free boundary conditions. Therefore, the *initial stress* field of a traction free finite crystal in equilibrium can be considered as a superposition of (a) the internal stress due to initial dislocation density distribution in the linear elastic infinite medium and (b) the image stress required to satisfy the traction-free boundary conditions. When an external stress is applied, the stress at any point in the finite body is a sum of the initial stress and the applied stress due to boundary conditions (again using superposition) at that point. In the regions having an initially prescribed dislocation density, less

applied stress is required to cause flow if both the initial stress and the applied stress are of the same sign as compared to the case when both are of opposite sign. Now, consider two cubic blocks of different sizes and same initial dislocation-density distribution. The magnitude of image stress corresponding to the $(1/r)$ fundamental stress field of a dislocation is higher for the smaller sample than the larger sample. Accordingly, in the case of the external applied stress being the same sign as the initial stress in the dislocation ‘core’ region, the smaller sample yields before the large sample (for a constant yield stress). If the sign of the initial dislocation density is now changed with the direction of applied stressing remaining the same, the initial stress changes sign, the larger sample has a smaller-in-magnitude initial stress that *subtracts* from the applied stress and consequently yields later than the smaller sample.

4. Conclusions

A finite element implementation of PMFDM has been shown to predict size effects at initial yield in micron-scale plasticity of single crystals. The results are qualitatively consistent with experimental observation in Uchic et al. (2004), Dimiduk et al. (2005) and Greer et al. (2005), as well as with recent discrete dislocation simulations of Weygand et al. (2007), Tang et al. (2007), Rao et al. (2008). In the PMFDM framework, size effects are caused by the internal stress of the dislocation distribution, its coupling to the imposed deformation conditions including deformation rate and, natural length scales that enter the theory through strain hardening and the ED velocity. However, an important observation from the computational experiments presented in this paper is that length scales associated with the internal stress due to discrete source patterns and those associated with the plastic strain rate of ED, are solely responsible for size effects at initial yield within this model. We observe a sensitivity of the mechanical response in the

presence of discrete source volumes or regions. Size-effect reversals under appropriate circumstances are also observed and explained.

Acknowledgments

We thank Armand Beaudoin for discussions on dynamical sensitivity. Support for this work from the National Science Foundation (Grant number: DMI-0423304), the Dowd-ICES Fellowship at CMU to Saurabh Puri, and the Metallic Materials Division of the AFRL at WPAFB is gratefully acknowledged.

References

- Acharya, A., 2001, A model of crystal plasticity based on the theory of continuously distributed dislocations, *Journal of the Mechanics and Physics of Solids* 49, 761- 785.
- Acharya, A., 2003, Driving forces and boundary conditions in continuum dislocation mechanics, *Proceedings of the Royal Society A* 459, 1343- 1363.
- Acharya, A., 2004, Constitutive analysis of finite deformation field dislocation mechanics, *Journal of the Mechanics and Physics of Solids* 52, 301- 316.
- Acharya, A., Beaudoin, A. J., 2000, Grain size effect in viscoplastic polycrystals at moderate strains, *Journal of the Mechanics and Physics of Solids* 48, 2213-2230.
- Acharya, A., Roy, A., 2006, Size effects and idealized dislocation microstructure at small scales: Predictions of a Phenomenological model of Mesoscopic Field Dislocation Mechanics: Part I, *Journal of the Mechanics and Physics of Solids* 54, 1687- 1710.

Balint, D. S., Deshpande, V. S., Needleman, A., Van der Giessen, E., 2006, Size effects in uniaxial deformation of single and polycrystals: a discrete dislocation plasticity analysis, *Modelling and Simulation in Materials Science and Engineering* 14, 409– 422.

Beaudoin, A. J., Acharya, A., Chen, S. R., Korzekwa, D. A., Stout, M. G., 2000, Consideration of grain-size effect and kinetics in the plastic deformation of metal polycrystals, *Acta Metallurgica* 48, 3409-3423.

Benzerga, A. A., Brechet, Y., Needleman, A., Van der Giessen, E., 2005, The stored energy of cold work: Predictions from discrete dislocation plasticity, *Acta Materialia* 53, 4765- 4779.

Benzerga, A. A., Shaver, N. F., 2006, Scale dependence of mechanical properties of single crystals under uniform deformation, *Scripta Materialia* 54, 1937– 1941.

Deshpande, V. S., Needleman, A., Van der Giessen, E., 2005, Plasticity Size effects in tension and compression of single crystals, *Journal of the Mechanics and Physics of Solids* 53, 2661- 2691.

Dimiduk, D. M., Uchic, M. D., Parthasarathy, T. A., 2005, Size-affected single-slip behavior of pure nickel microcrystals, *Acta Materialia* 53, 4065– 4077.

Fleck, N. A., Muller, G. M., Ashby, M. F., Hutchinson, J. W., 1994, Strain gradient plasticity: theory and experiment, *Acta Metallurgica et Materialia* 42, 475– 487.

Greer, J. R., Oliver, W. C., Nix, W. D., 2005, Size dependence of mechanical properties of gold at the micron scale in the absence of strain gradients, *Acta Materialia* 53, 1821- 1830.

Ma, Q., Clarke, D. R., 1995, Size-dependent hardness of silver single-crystals, *Journal of Materials Research* 10 (4), 853– 863.

Norfleet, D. M., Dimiduk, D. M., Polasik, S. J., Uchic, M. D., Mills, M. J., 2008, Examination of Dislocation Structures and Their Relationship to Strength of Pure Nickel Microcrystals, *Acta Materialia*, submitted for publication.

Nye, J. F., 1953, Some geometrical relations in dislocated crystals, *Acta Metallurgica* 1, 153-162

Parthasarathy, T. A., Rao, S. I., Dimiduk, D. M., Uchic, M. D., Trinkle, D. R., 2006, Contribution to size effect of yield strength from the stochastics of dislocation source lengths in finite samples, *Scripta Materialia* 56, 313-316.

Rao, S. I., Dimiduk, D. M., Parthasarathy, T. A., Uchic, M. D., Tang, M., Woodward, C., 2008, Athermal mechanisms of size-dependent crystal flow gleaned from three dimensional discrete dislocation simulations, *Acta Materialia*, submitted for publication.

Roy, A., Acharya, A., 2006, Size effects and idealized dislocation microstructure at small scales: Predictions of a Phenomenological model of Mesoscopic Field Dislocation Mechanics: Part II, *Journal of the Mechanics and Physics of Solids* 54, 1711- 1743.

Stölken, J. S., Evans, A. G., 1998, A microbend test method for measuring the plasticity length scale, *Acta Materialia* 46 (14), 5109-5115.

Tang, H., Schwarz, K. W., Espinosa, H. D., 2007, Dislocation escape-related size effects in single-crystal micropillars under uniaxial compression, *Acta Materialia* 55, 1607- 1616.

Uchic, M. D., Dimiduk, D. M., Florando, J. N., Nix, W. D., 2004, Sample dimensions influence strength and crystal plasticity, *Science* 305, 986-989.

Varadhan, S. N., Beaudoin, A. J., Acharya A., Fressengeas, C., 2006, Dislocation transport using an explicit Galerkin/least-squares formulation, *Modelling and Simulation in Materials Science and Engineering* 14, 1245-1270.

Weygand, D., Poignant, M., Gumbsch, P., Kraft, O., 2007, Three-dimensional dislocation dynamics simulation of the influence of sample size on the stress–strain behavior of fcc single-crystalline pillars, Mater. Sci. Engr. A, in press

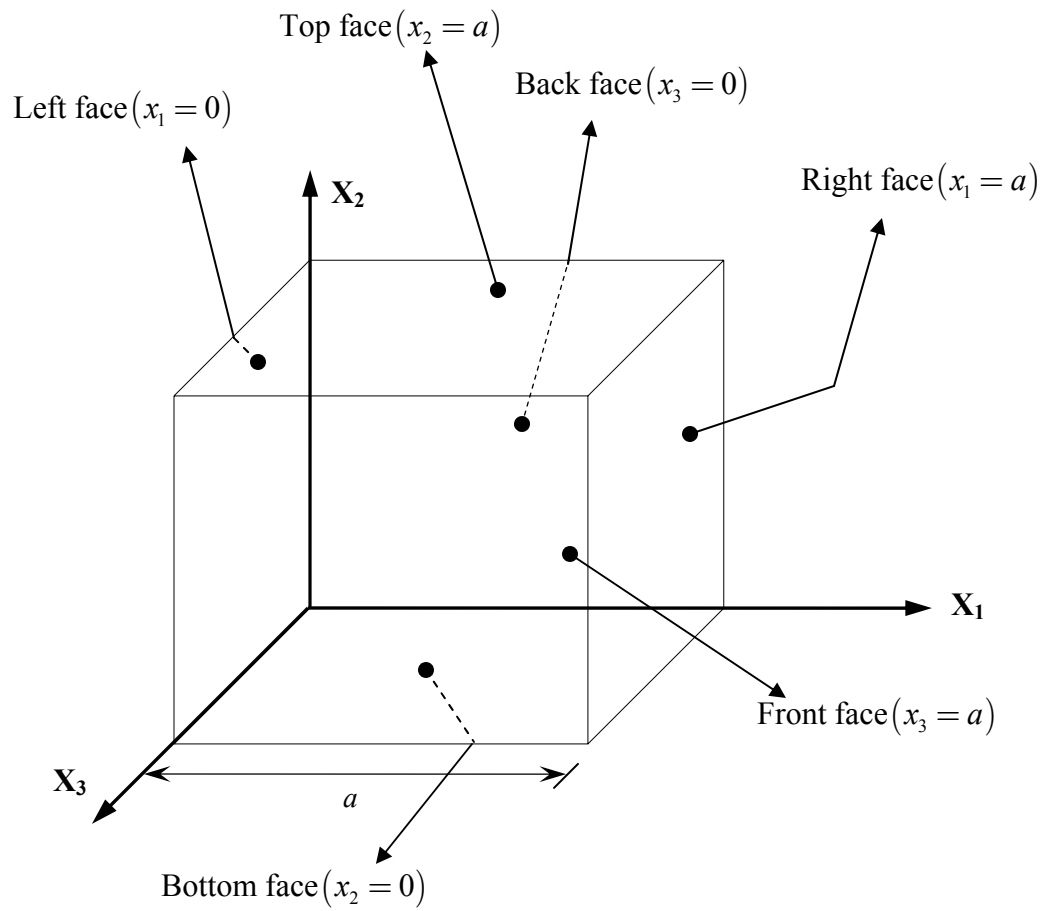


Figure. 1. Schematic layout of a typical model geometry.

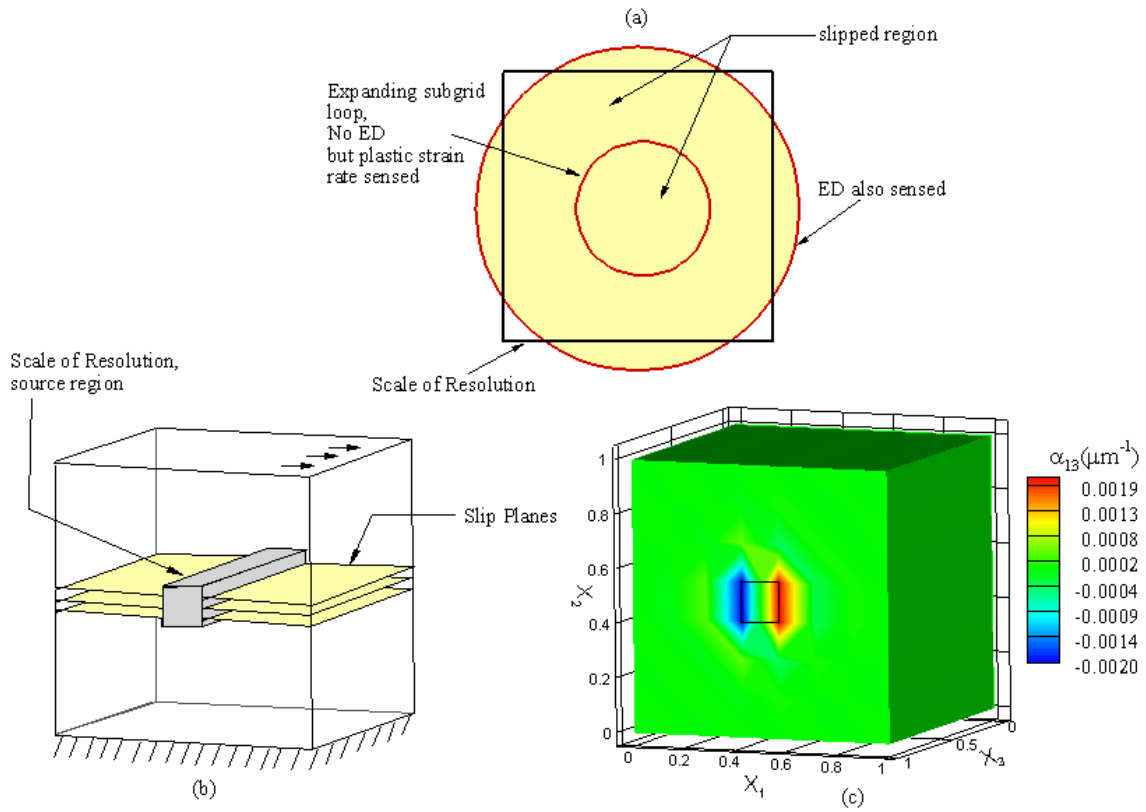


Figure 2. (a) Physical representation of a Frank Read source; (b) Representation of a numerically simulated Frank Read Source; (c) Excess dislocation density at $\Gamma = 0.1\%$ for pattern (a)

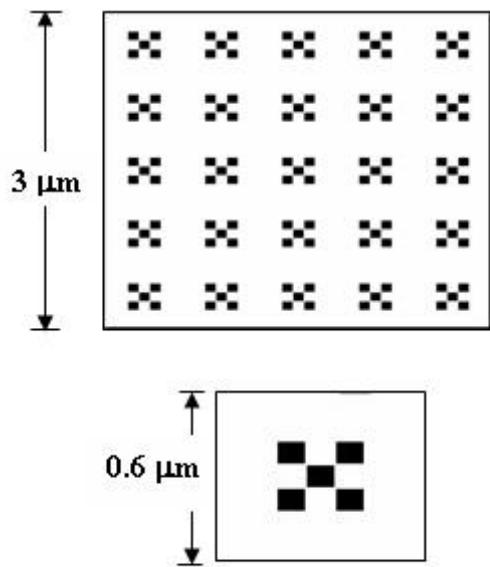


Figure 3. Schematic layout of position of sources (Black spots represents the dislocation sources)

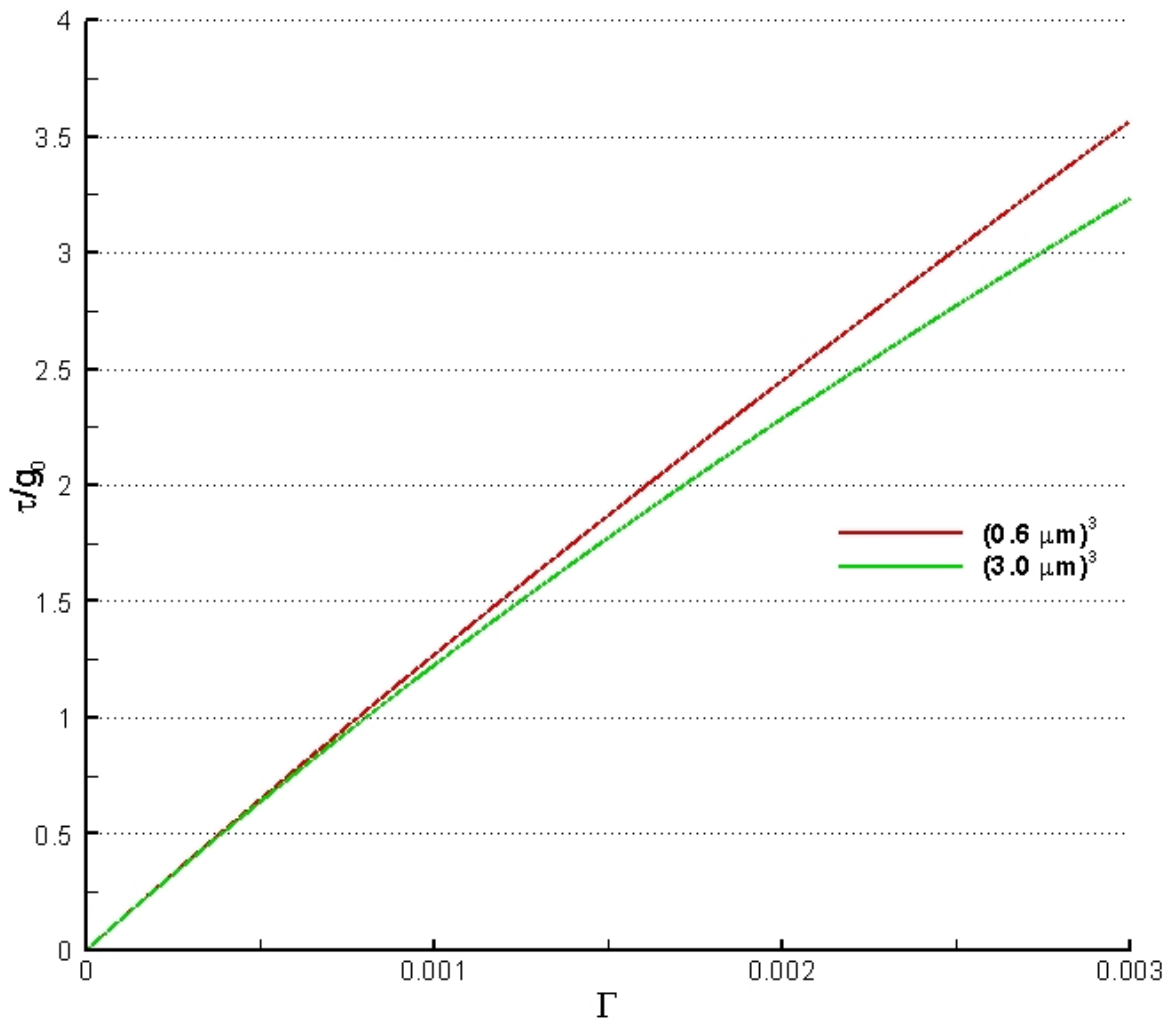
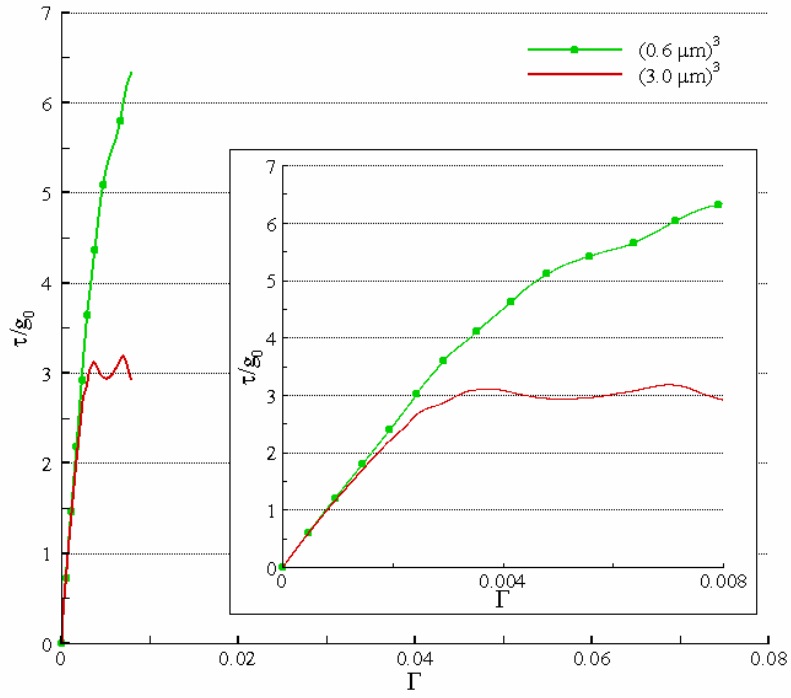
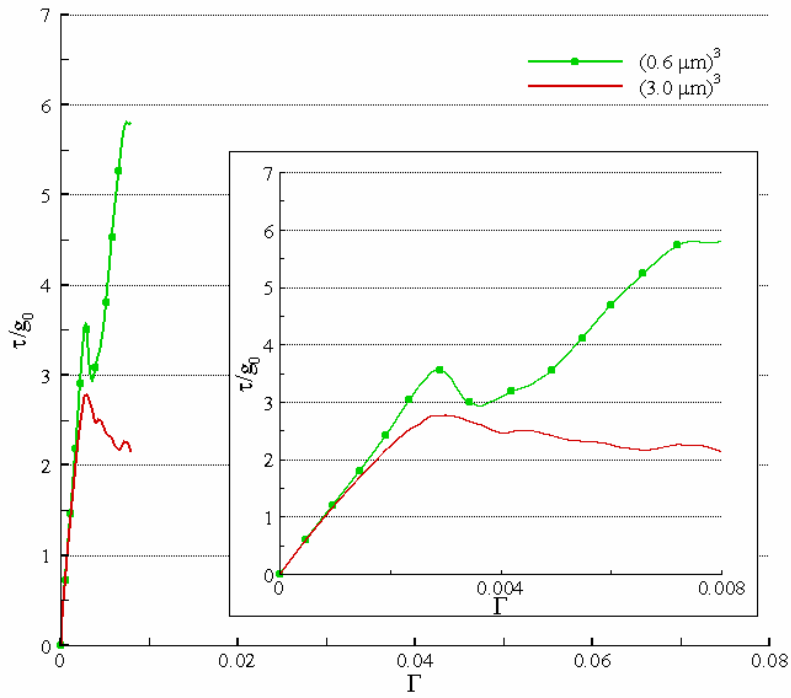


Figure 4. Size effect in simple shear with a predefined spatial distribution of dislocation sources, within a conventional plasticity framework.



(a)



(b)

Figure 5. Size effect in simple shear with a predefined source pattern with: (a) equation (15) used for hardening rate, (b) equation (22) used for hardening rate.

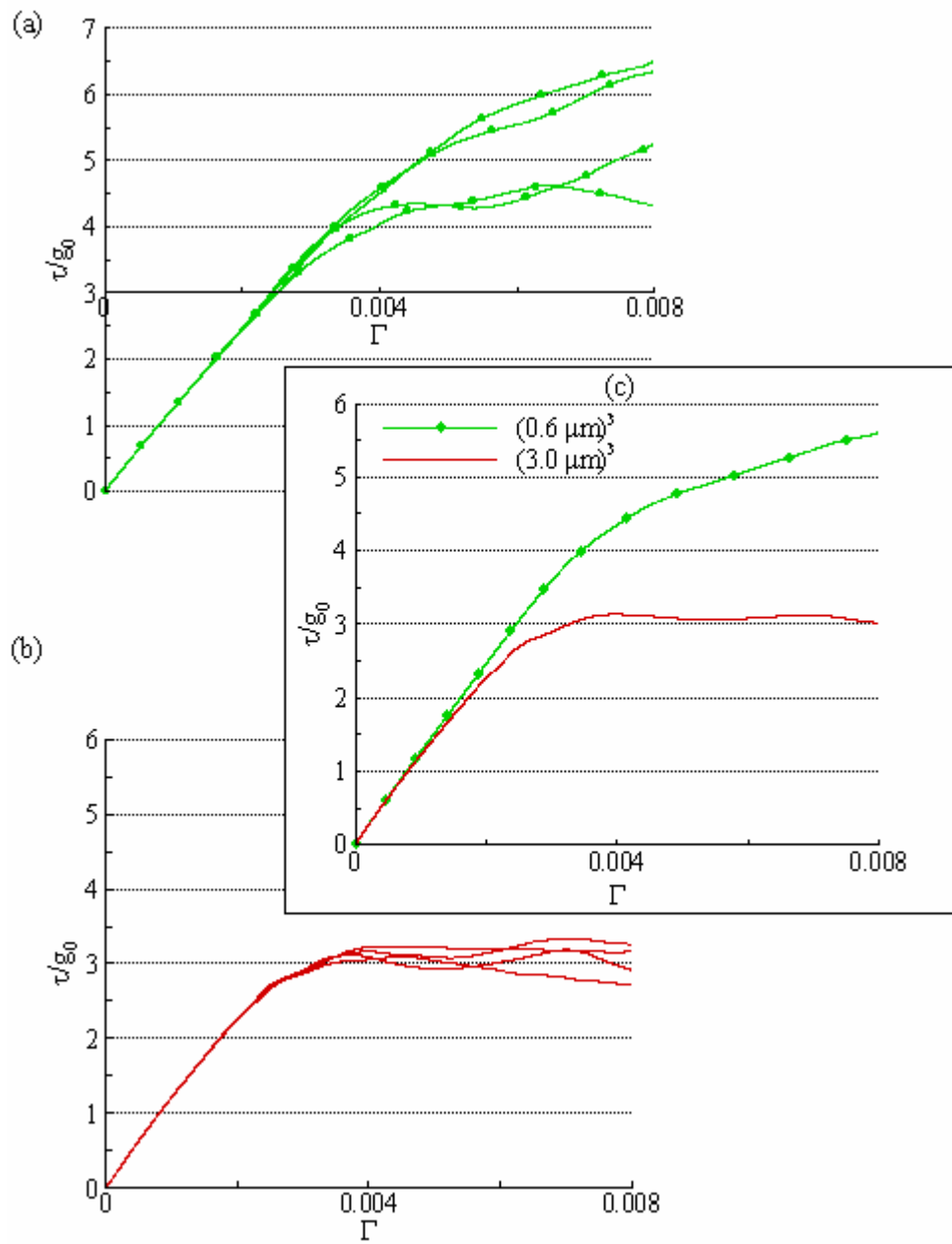


Figure 6. Variability in stress-strain response in simple shear with perturbation in boundary conditions: (a) $0.6 \mu\text{m}$, (b) $3.0 \mu\text{m}$ and (c) Mean response for the two sizes

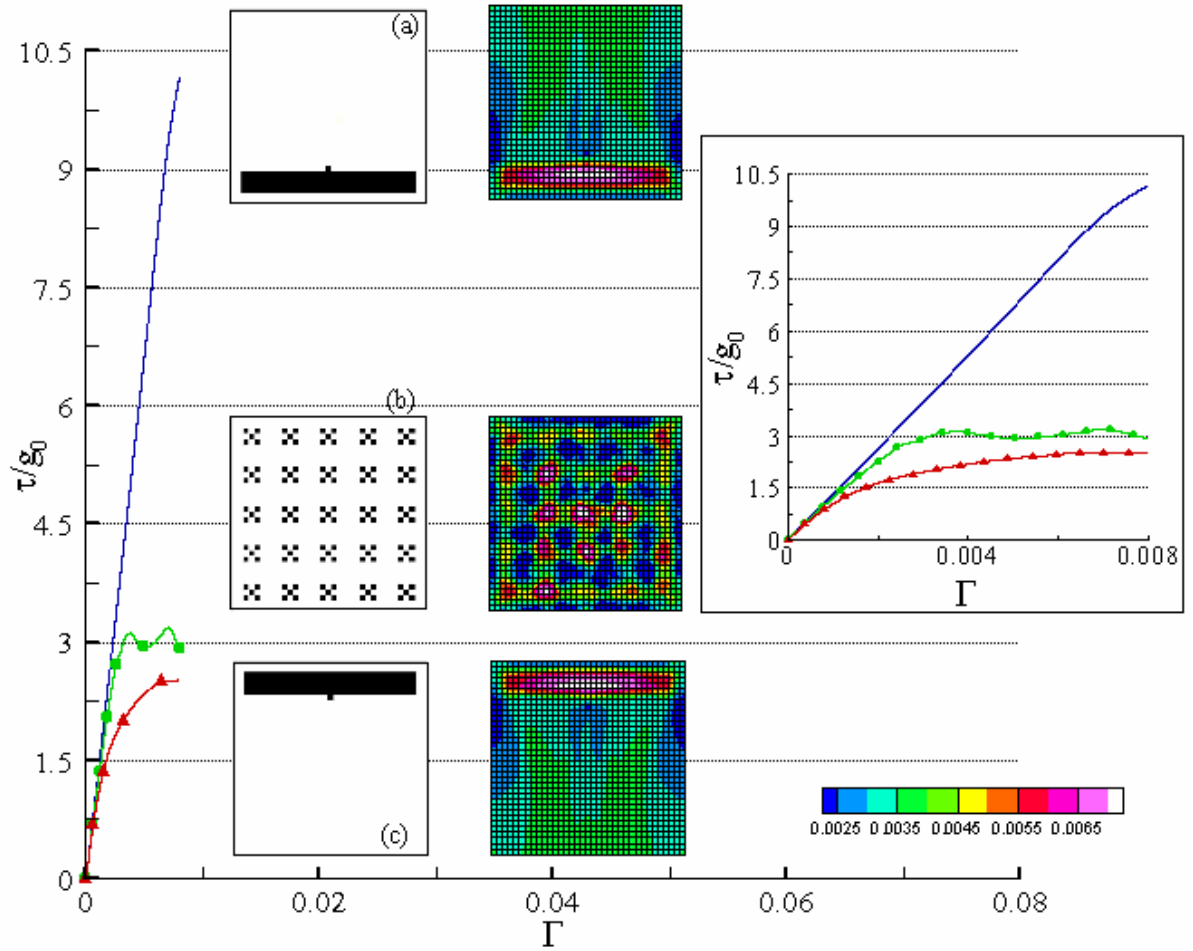
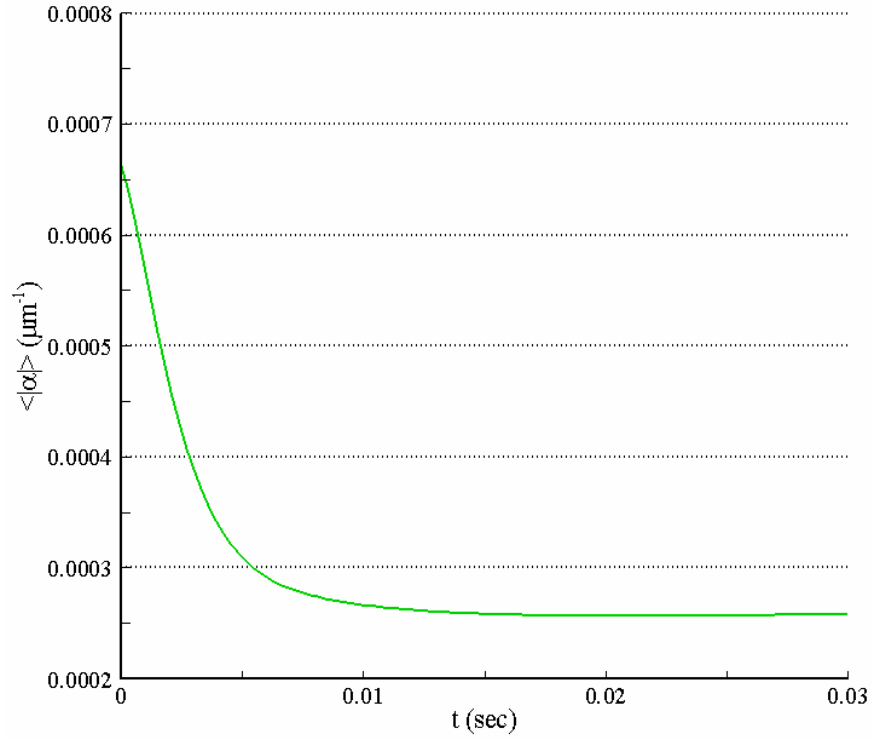
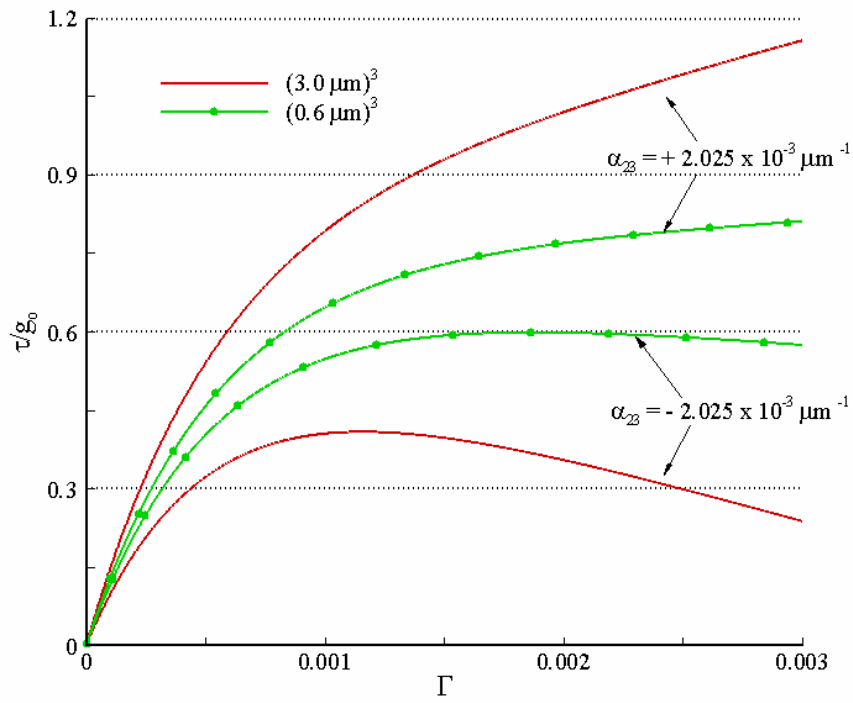


Figure 7. Variability in stress-strain response with change in the source pattern.



(a)



(b)

Figure 8. (a) Variation in average of $|\alpha|$ over the whole domain with time, (b) Size effect in simple shear with a non- zero initial ED density.

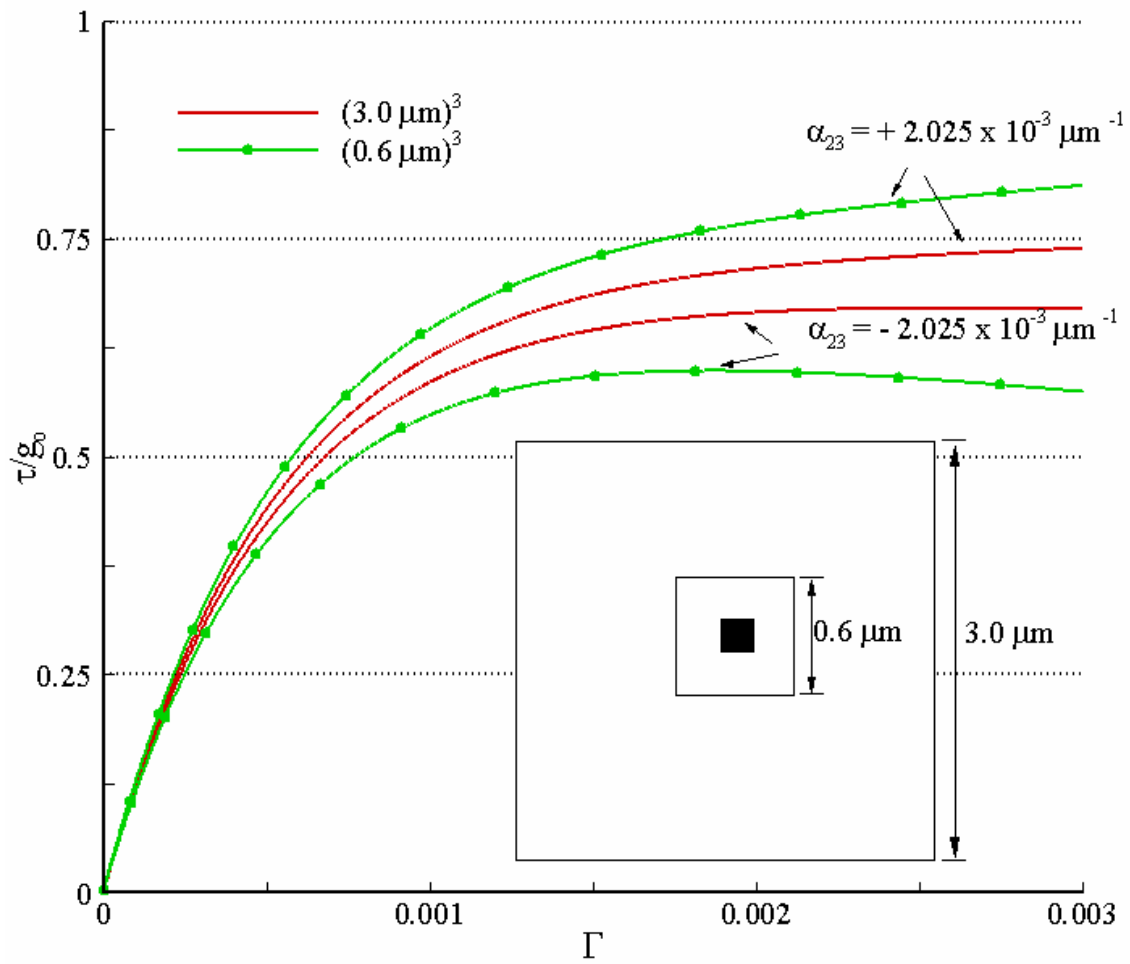


Figure 9. Size effect in simple shear with a non- zero initial ED density and the new pattern as shown in the inset